Deciphering sex-specific genetic architectures using local Bayesian regressions

Scott A Funkhouser[1¶], Ana I Vazquez[2], Juan P Steibel[3], Catherine W Ernst[3], Gustavo de los Campos[2*¶]

[1] Genetics Graduate Program, Michigan State University, East Lansing, Michigan, United States

[2] Departments of Epidemiology & Biostatistics and Statistics & Probability, Institute for Quantitative Health Science and Engineering, Michigan State University, East Lansing, Michigan, United States

[3] Department of Animal Science, Michigan State University, East Lansing, Michigan, United States

* Corresponding author

E-mail: gustavoc@msu.edu

[¶]These authors contributed equally to this work.

Abstract

Many complex human traits exhibit differences between sexes. While numerous factors likely contribute to this phenomenon, growing evidence from genome-wide studies suggest a partial explanation: that males and females from the same population possess differing genetic architectures. Despite this, mapping gene-by-sex (G×S) interactions remains a challenge likely because the magnitude of such an interaction is typically and exceedingly small; traditional genome-wide association techniques may be underpowered to detect such events partly due to the burden of multiple test correction. Here, we developed a local Bayesian regression (LBR) method to estimate sex-specific SNP marker effects after fully accounting for local linkage-disequilibrium (LD) patterns. This enabled us to infer sex-specific effects and G×S interactions either at the single SNP level, or by aggregating the effects of multiple SNPs to make inferences at the level of small LD-based regions. Using simulations in which there was imperfect LD between SNPs and causal variants, we showed that aggregating sex-specific marker effects with LBR provides improved power and resolution to detect G×S interactions over traditional single-SNP-based tests. When using LBR to analyze traits from the UK Biobank, we detected a relatively large G×S interaction impacting bone-mineral density within *ABO* and replicated many previously detected large-magnitude G×S interactions impacting waist-to-hip ratio. We also discovered many new G×S interactions impacting such traits as height and BMI within regions of the genome where both male- and female-specific effects explain a small proportion of phenotypic variance ($R^2 < 1x10^{-4}$), but are enriched in known expression quantitative trait loci. By combining biobank-level data and techniques to estimate sex-specific SNP effects after accounting for local-LD patterns, we are providing evidence that numerous small-magnitude G×S interactions exist to influence sex differences in a variety of complex traits.

Author Summary

Many complex human traits are known to be influenced by an impressive number of causal variants each with very small effects, posing great challenges for genome-wide association studies (GWAS). To add to this challenge, many causal variants may possess context-dependent effects such as effects that are dependent on biological sex. While GWAS are commonly performed using specific methods in which one single nucleotide polymorphism (SNP) at a time is tested for association with a trait, alternatively we utilize methods more commonly observed in the genomic prediction literature. Such methods are advantageous in that they are not burdened by multiple test correction in the same way as traditional GWAS techniques are, and can fully account for linkage-disequilibrium patterns to accurately estimate the true effects of SNP markers. Here we adapt such methods to estimate genetic effects within sexes and provide a powerful means to compare sex-specific genetic effects.

Introduction

Sex differences are widespread in nature, observed readily among many human traits and diseases. For quantitative traits, sex may affect the distribution of phenotypes at various levels, including mean-differences between genetic males and genetic females (hereafter referred to as males and females, respectively) as well as differences in variance. Sex differences are likely due to a myriad of factors including differential environmental exposures, unequal gene dosages for sex-linked genes as well as sex-heterogeneity in the architecture of genetic effects at one or more autosomal loci (i.e. gene-by-sex (G×S) interactions). In this way, sex is considered an

environmental variable, providing two well-defined conditions in which allele frequencies and linkage disequilibrium (LD) patterns are equivalent but nevertheless genetic effects of one or many autosomal loci may differ.

Evidence for different genetic architectures between sexes among human populations is largely supported by genome-wide parameters [1–4] including unequal within-sex heritabilities ($h^2_{\text{male}} \neq h^2_{\text{female}}$) and between-sex genetic correlations less than one ($r_g < 1$); the former suggests that the proportion of phenotypic variance explained by genetic factors varies between sexes, while the latter suggests genetic effects are disproportional between sexes [5]. Although many traits seem to have between-sex genetic correlation that is evidentially less than one, genome-wide association (GWA) studies intended to map G×S interactions have struggled to pinpoint such loci [6,7]. Based on this dichotomy, G×S interactions presumably exist for many traits, but the magnitude of a typical G×S interaction is suspected to be exceedingly small, explaining why such events commonly elude detection, particularly after multiple test correction. However, just as numerous small effect causal loci accumulate to affect phenotypic variance, small G×S interactions may accumulate to influence both sex differences and phenotypic variance.

Most GWA studies utilize single-marker regression (SMR), in which the phenotype is regressed upon allele content one SNP at a time, thereby obtaining marginal SNP effect size estimates that do not fully account for LD patterns. In contrast, whole-genome regression methods, in which the phenotype is regressed upon all SNPs across the genome concurrently, fully account for multi-locus LD. These methods are increasingly being used as a one-stop solution to estimate true (conditional) effect sizes of SNP markers and to provide genome-wide estimates including genomic heritability [8–10] and between-sex genetic correlations [2–4]. By estimating true SNP effect sizes, the goal across many studies is to select SNPs with non-zero

85 effects and to build a model for predicting polygenic scores [11–13]. Other works have directly
86 illustrated the use of whole-genome regression methods for GWAS [14–17]. Whole-genome
87 regressions are computationally challenging to use with biobank-level data; however, recent
88 work suggests relatively accurate genomic prediction and SNP effect estimation can be achieved
89 by simply accounting for local LD patterns (as opposed to global LD patterns) [18].

90 Building on the idea of utilizing true SNP marker effects, here we developed local
91 Bayesian regressions (LBR) in which the phenotype is regressed upon multiple SNPs spanning
92 multiple LD blocks (thereby accounting for local LD patterns) to study sex differences in
93 complex traits from the UK Biobank. The LBR model uses random-effect SNP-by-sex
94 interactions [19,20] that decompose conditional SNP effects into three components: i) one shared
95 across sexes, ii) a male-specific deviation from the shared component, and iii) a female-specific
96 deviation from the shared component. Using samples from the posterior distribution of
97 conditional SNP effects, we developed methods to infer sex-specific effects and G×S interactions
98 at the single SNP level and by aggregating SNP effects within small LD-based regions, offering
99 multiple perspectives to study sex-specific genetic architectures.

100 In this study, we have utilized genotypes for 607,497 autosomal SNPs from ~259,000
101 distantly related Caucasians from the UK Biobank for assessing LBR's performance in analyzing
102 simulated and real complex traits including height, BMI, waist-to-hip ratio (WHR), and heel
103 bone-mineral density (BMD). Simulations showed that (i) for inferences of G×S interactions,
104 LBR offers higher power with lower FDR than methods based on marginal effects (aka single-
105 marker regression) and (ii) we show that under imperfect LD between SNPs and causal variants
106 (i.e., when causal variants are not genotyped), aggregating SNP effects within small LD-based
107 regions offers higher power than methods based on testing individual SNPs.

The traits analyzed in this study span a range of genome-wide metrics and G×S suggestibility; from height and BMI for which previous studies indicate males and females possess very similar genetic architectures [3], to WHR, a trait with well-documented G×S interactions [21–24], and BMD, for which G×S interactions are thought to exist but have eluded detection [25]. LBR provided evidence of G×S interactions impacting height, BMI, and BMD at regions of the genome where sex-specific genetic effects are relatively small, however such regions are enriched in known eQTL. For WHR, LBR replicated many large-magnitude G×S interactions previously discovered using single-marker regression, but also located novel G×S interactions near such genes as the estrogen receptor *ESR1*.

Results

Overview of the LBR model, inference methods, and implementation

To study sex differences we regressed male and female phenotypes ($\boldsymbol{y}_{\mathrm{m}}$ and $\boldsymbol{y}_{\mathrm{f}}$) on male and female genotypes ($\boldsymbol{X}_{\mathrm{m}}$ and $\boldsymbol{X}_{\mathrm{f}}$) using a SNP-by-sex interaction model of the form

$$\begin{bmatrix}\boldsymbol{y}_{\mathrm{m}}\\ \boldsymbol{y}_{\mathrm{f}}\end{bmatrix}=\begin{bmatrix}\mathbf{1}\mu_{\mathrm{m}}\\ \mathbf{1}\mu_{\mathrm{f}}\end{bmatrix}+\begin{bmatrix}\boldsymbol{X}_{\mathrm{m}}\\ \boldsymbol{X}_{\mathrm{f}}\end{bmatrix}\boldsymbol{b}_0+\begin{bmatrix}\boldsymbol{X}_{\mathrm{m}}\\ \mathbf{0}\end{bmatrix}\boldsymbol{b}_{\mathrm{m}}+\begin{bmatrix}\mathbf{0}\\ \boldsymbol{X}_{\mathrm{f}}\end{bmatrix}\boldsymbol{b}_{\mathrm{f}}+\begin{bmatrix}\boldsymbol{\varepsilon}_{\mathrm{m}}\\ \boldsymbol{\varepsilon}_{\mathrm{f}}\end{bmatrix}.\#(1)$$

Above, μ_{m} and μ_{f} are male and female intercepts, $\boldsymbol{b}_0=\left\{b_{0_j}\right\}$ (j = 1, … , p) is a vector of main effects, $\boldsymbol{b}_{\mathrm{m}}=\left\{b_{\mathrm{m}_j}\right\}$ and $\boldsymbol{b}_{\mathrm{f}}=\left\{b_{\mathrm{f}_j}\right\}$ are male and female interactions, respectively and $\boldsymbol{\varepsilon}_{\mathrm{m}}=\left\{\varepsilon_{\mathrm{m}_i}\right\}$ and $\boldsymbol{\varepsilon}_{\mathrm{f}}=\left\{\varepsilon_{\mathrm{f}_i}\right\}$ are male and female errors which were assumed to follow normal distributions with zero mean and sex-specific variances. Female-specific and male-specific SNP effects are defined as $\beta_{\mathrm{f}_j}=b_{0_j}+b_{\mathrm{f}_j}$ and $\beta_{\mathrm{m}_j}=b_{0_j}+b_{\mathrm{m}_j}$, respectively.

Prior assumptions. For SNP effects we adopted priors from the spike-slab family with a point of mass at zero and a Gaussian slab [26] specifically, $p\left(b_{k_j}\right) = \pi_k N\left(0, \sigma^2_{b_k}\right) + (1 - \pi_k)1\left(b_{k_j} = 0\right)$ (where $k = 0$, f or m). Here, π_k and $\sigma^2_{b_k}$ are hyper-parameters representing the proportion of nonzero effects and the variance of the slab; these hyper-parameters were treated as unknown and given their own hyperpriors (see Methods).

Local-regression. Implementing the above model with whole-genome SNPs (p ~ 600K) and very large sample size (n ~ 300K) is computationally extremely challenging. However, LD in homogeneous un-structured human populations spans over relatively short regions (R^2 between allele dosages typically vanishes within 1-2 Mb; S1 Fig). Therefore, we applied LBR to long, overlapping chromosome segments (Fig. 1). Specifically, we divided the genome into "core" segments containing 1,500 contiguous SNPs (roughly 8Mb, on average), then applied the regression in equation (1) to SNPs in the core segment plus 250 SNPs (i.e., roughly 1Mb) in each flanking region, which were added to account for LD between SNPs at the edge of each core segment with SNPs in neighboring segments.

Inferences. We used the BGLR [27] software to draw samples from the posterior distribution of the model parameters and used these samples to make inference about individual SNP effects including: (i) the posterior probability that the j^{th} SNP has a nonzero effect in males ($\text{PPM}_{\text{SNP}_j}$) and females ($\text{PPF}_{\text{SNP}_j}$) and (ii) the posterior probability that the female and male effects are different ($\text{PPDiff}_{\text{SNP}_j}$).

In regions involving multiple SNPs in strong LD, inferences at the individual-SNP level may be questionable. Therefore we borrowed upon previous work by Fernando et al. [14],

enabling us to aggregate multiple sex-specific SNP effects within relatively small regions using "window variances". For each SNP j we defined a window j^* around the SNP based on local LD patterns (see Methods). We then defined the male-specific and female-specific window variances as $\sigma^2_{g_{\mathrm{m}\,j^*}} = var\left(\boldsymbol{X}_{j^*}\boldsymbol{\beta}_{\mathrm{m}_{j^*}}\right)$ and $\sigma^2_{g_{\mathrm{f}\,j^*}} = var\left(\boldsymbol{X}_{j^*}\boldsymbol{\beta}_{\mathrm{f}_{j^*}}\right)$, respectively. Here, $\boldsymbol{X}_{j^*}$ represent genotypes at SNPs within the j^* window and $var(\quad)$ is the sample variance operator. Prior to model fitting, the phenotype is scaled across sexes; thus, sex-specific window variances may be interpreted as the proportion of total phenotypic variance explained by sex-specific SNP effects. From samples of sex-specific window variances, we computed the posterior probability of (i) nonzero male-specific window variance ($\mathrm{PPM}_{\sigma^2_{g_{j*}}}$), (ii) nonzero female-specific window variance ($\mathrm{PPF}_{\sigma^2_{g_{j*}}}$), and (iii) sex difference in window variances (denoted as $\mathrm{PPDiff}_{\sigma^2_{g_{j*}}}$).

Local Bayesian regressions offer improved power with lower false-discovery rates

We used simulations to assess the power and false discovery rate (FDR) of LBR and to compare it with that of standard single-marker-regression (SMR). Traits were simulated using SNP genotypes from the Axiom UK-Biobank (119,190 males and 139,738 females, all distantly related Caucasians). We simulated a highly complex trait with one causal variant (CV) per ~2Mb which on average explained a proportion of the phenotypic variance equal to $3.3\text{x}10^{-4}$. Our simulation used a total of 60,000 SNPs (consisting of 6,000 consecutive SNPs taken from 10 different chromosomes) and 150 CVs; on the complete human genome "scale" this corresponds to a trait with 1,500 CVs and a heritability of 0.5 (see Methods for further details). 40% of the

CVs (a total of 60 SNPs in our simulation) had differing sex-specific effects and the remaining 60% (90 SNPs) had effects that were the same in males and females.

Power and FDR when causal variants are genotyped. First, we analyzed the simulated phenotypes using all SNPs (including the 150 causal ones). Initially interested in inferring G×S interactions, we ranked SNPs based on LBR's $\mathrm{PPDiff}_{\mathrm{SNP}_j}$ metric and based on SMR's *p*-value for sex difference (*pvalue*-diff , see Methods) and used the two ranks to estimate power and FDR as a function of the number of SNPs selected (Fig 2). LBR showed consistently higher power (achieving a power of ~80% when selecting the top 50 SNPs with highest $\mathrm{PPDiff}_{\mathrm{SNP}_j}$) and lower FDR than SMR. The false discovery rate of LBR was very low when selecting the top-50 SNPs with highest $\mathrm{PPDiff}_{\mathrm{SNP}_j}$ and exhibited a very sharp phase-transition with fast increase in FDR thereafter.

We also compared the two methods based on arbitrary, albeit commonly used, mapping thresholds for SMR and LBR. At $\mathrm{PPDiff}_{\mathrm{SNP}_j} \geq 0.95$, LBR selected an average (across simulation replicates) of 38.33 SNPs with an estimated power of 0.634 and estimated FDR of 0.007. Conversely, at *pvalue*-diff $\leq 5\mathrm{x}10^{-8}$, SMR selected an average of 50.7 SNPs with an estimated power of 0.436 and estimated FDR of 0.451. Altogether, these results suggest that for G×S discovery, LBR offers higher power and lower FDR than SMR—the method most widely used in GWA studies—at least when G×S interactions are observed.

When trying to map SNPs that had effect in at least one sex, we used $\mathrm{PP}_{\mathrm{SNP}_j} = \max\left[\mathrm{PPM}_{\mathrm{SNP}_j}, \mathrm{PPF}_{\mathrm{SNP}_j}\right]$ and *p*-values from an F-test (see Methods) as metrics for LBR and SMR methods, respectively. Again, LBR showed higher power with lower FDR than a standard SMR *p*-value (S1 Fig). At traditional mapping thresholds, LBR and SMR had similar power but

LBR achieved that power with much lower FDR; at $PP_{SNP_j} \geq 0.95$, the average number of SNPs selected was 120.83 with an estimated power of 0.799 and estimated FDR of 0.009 while at *p*-value $\leq 5x10^{-8}$, the number of SNPs selected was 374.56 with an estimated power of 0.794 and FDR of 0.66.

Power and FDR under imperfect LD. In a second round of analyses, we removed all CVs from the panel of SNPs used in the analysis to represent a situation where CVs are not observed, and genotyped SNPs are tagging CVs at varying degrees. As before, we initially assessed the relative performance of LBR to infer segments harboring G×S interactions. Power and FDR were assessed at several resolutions: 1Mb, 500Kb and 250Kb regions around each CV. At each resolution, a discovery was considered true if the finding laid within a segment harboring a G×S CV. Power and FDR were computed at different thresholds ($PPDiff_{SNP_j}$ and $PPDiff_{\sigma^2_{\tilde{g}_{j*}}}$ for LBR and *pvalue*-diff for SMR; Fig 3). When using a 1Mb target area—such that correct G×S discoveries must be within 500Kb on either side of a true G×S event—$PPDiff_{\sigma^2_{\tilde{g}_{j*}}}$ thresholds (LBR's window-based metrics) provided highest power within an FDR range of 0-0.3, thereafter SMR provided slightly higher power. As expected, when removing CVs, power was estimated to be much lower than when CVs were observed; at $PPDiff_{\sigma^2_{\tilde{g}_{j*}}} \geq 0.95$, the estimated power and FDR were 0.454 and 0.004, respectively, while at *pvalue*-diff $\leq 5x10^{-8}$, estimated power and FDR were 0.22 and 0.006. As seen in Fig 3, when considering a finer resolution (500Kb and 250Kb) the performance of both LBR-based approaches was more robust than SMR. Altogether this indicates that for the discovery and mapping of unobserved G×S interactions, LBR's window-based metric provides higher power with equivalent FDR and finer resolution than single-marker regression methods.

To infer segments containing CVs that affect at least one sex, we again used LBR to decide whether either sex-specific effect was nonzero at the level of individual SNPs or windows. Using a 1MB target area, LBR's window-based metrics provided the highest power within an FDR range of 0-0.025. When decreasing the target area, LBR provided the highest power over larger FDR ranges (S2 Fig).

For real human traits, many newly discovered G×S interactions show relatively small sex-specific effects

We analyzed four complex human traits (height, BMI, BMD, and WHR) measured among ~259,000 distantly related Caucasians from the UK Biobank (~119,000 males and ~140,000 females). For each trait, we fit the LBR model (eq. 1) across the entire autosome consisting of 607,497 genotyped SNPs using 417 overlapping segments (Fig. 1) and obtained evidence of G×S interactions at the level of SNP j and window j^*.

To compare both the magnitude and sign of sex-specific SNP effects, we plotted each $\hat{\beta}_{\mathrm{f}_j}$ against $\hat{\beta}_{\mathrm{m}_j}$ (Fig 4a). The trait was scaled across sexes prior to model fitting; thus, male- and female- specific effects were not constrained to the same scale. In this way, one might expect male-specific SNP effects to uniformly differ from female-specific SNP effects by a multiplicative factor if the variance of the phenotype is different between sexes (sample statistics within each sex are provided within S1 Table). Surprisingly, we did not observe evidence of sex-specific SNP effects uniformly differing due to differences in phenotypic scale; for height, BMD, and BMI, as seen in Fig. 4a, most large effect SNPs lie near the blue diagonal line. For WHR, we observed largely consistent results from prior studies [21–23]: namely the prevalence of

numerous SNPs with relatively large effects in females but little to no effect in males. No traits exhibited evidence of any SNPs with (i) high confidence male- and female- specific effects (no SNPs with $\mathrm{PPM}_{\mathrm{SNP}_j} \geq 0.9$ and $\mathrm{PPF}_{\mathrm{SNP}_j} \geq 0.9$) and (ii) differing signs between sexes.

We then aggregated sex-specific SNP effects within small LD-based regions to estimate sex-specific window variances $\sigma^2_{g_{\mathrm{m}j^*}}$ and $\sigma^2_{g_{\mathrm{f}j^*}}$ and compared the magnitude of each (Fig 4b). Interestingly for traits such as height, many large effect regions bear slightly larger window variances for males than for females. This was not observed at the single SNP level, suggesting that many regions bearing numerous small effect SNPs produce aggregate effects that are potentially larger (although not reaching a $\mathrm{PPDiff}_{\sigma^2_{g_{j^*}}} \geq 0.9$ threshold) in males than in females. One example is the GDF5 locus, previously known to strongly associate with adult height [28], where a peak $\mathrm{PPDiff}_{\sigma^2_{g_{j^*}}}$ signal centered on rs143384 had slightly different estimated sex-specific window variances ($\hat{\sigma}^2_{g_{\mathrm{m}j^*}} = 3.0\mathrm{x}10^{-3}$ and $\hat{\sigma}^2_{g_{\mathrm{f}j^*}} = 2.6\mathrm{x}10^{-3}$) but weak evidence of a G×S interaction ($\mathrm{PPDiff}_{\sigma^2_{g_{j^*}}} = 0.544$). For BMD, several large effect regions show suggestive evidence of G×S interactions including the *AKAP11* locus and the *CCDC170* locus ($\mathrm{PPDiff}_{\sigma^2_{g_{j^*}}} = 0.856$ and 0.745, respectively), both previously associated with bone mineral density [29–32].

To make G×S inferences at the level of window variances irrespective of the magnitude of sex-specific effects, we adopted a $\mathrm{PPDiff}_{\sigma^2_{g_{j^*}}}$ threshold of 0.9, which in simulations (Fig 3) provided optimal power at an estimated FDR of 0.029 when using a 1MB target area. For height, a total of eight distinct regions possessed a $\mathrm{PPDiff}_{\sigma^2_{g_{j^*}}} \geq 0.9$, two of which possessed a $\mathrm{PPDiff}_{\sigma^2_{g_{j*}}} \geq 0.95$. For BMI, 5 distinct regions possessed a $\mathrm{PPDiff}_{\sigma^2_{g_{j*}}} \geq 0.9$ with none reaching a more stringent $\mathrm{PPDiff}_{\sigma^2_{g_{j*}}} \geq 0.95$ threshold, and none overlapping with two previously suggested BMI

G×S SNPs [33]. As seen in Fig 4C, inferred G×S interactions for height and BMI possess relatively small sex-specific window variances; as an example, for height, the window centered on SNP rs1535515 (near *LRRC8C*) had a $\text{PPDiff}_{\sigma^2_{g_{j^*}}} = 0.96$, while $\hat{\sigma}^2_{g_{\text{m}_{j^*}}} = 2.1\text{x}10^{-5}$ and $\hat{\sigma}^2_{g_{\text{f}_{j^*}}} = 1.1\text{x}10^{-4}$. For BMD, seven regions reached a 0.9 $\text{PPDiff}_{\sigma^2_{g_{j^*}}}$ threshold while one higher-confidence G×S interaction ($\text{PPDiff}_{\sigma^2_{g_{j^*}}} \geq 0.95$) was detected within *ABO*, the gene controlling blood type.

For WHR, roughly 45 distinct genomic regions possessed a $\text{PPDiff}_{\sigma^2_{g_{j^*}}} \geq 0.9$, while 34 of these possessed a $\text{PPDiff}_{\sigma^2_{g_{j^*}}} \geq 0.95$. We found many previously detected G×S interactions known to associate with WHR or a related trait, WHR adjusted for BMI (WHRadjBMI) [21–24]. These included interactions at *LYPLAL1*, *MAP3K1*, *COBLL1*, *RSPO3*, and *VEGFA* among others. We also detected numerous novel G×S interactions (Table 1) near physiologically intriguing genes such as the estrogen receptor gene *ESR1* and the ATP binding cassette transporter A1 gene *ABCA1* known to play a role in HDL metabolism ($\text{PPDiff}_{\sigma^2_{g_{j^*}}} \geq 0.95$). As seen in Table 1, both novel signals possessed a high-confidence female-specific effect with weak evidence for a male-specific effect ($\text{PPF}_{\sigma^2_{g_{j^*}}} \geq 0.95$; $\text{PPM}_{\sigma^2_{g_{j^*}}} \leq 0.6$), however the magnitude of the female-specific effect was relatively small ($\hat{\sigma}^2_{g_{\text{f}_{j^*}}} \leq 1.4\text{x}10^{-4}$). As evident from Table 1, most novel WHR G×S interactions detectable with LBR are those with relatively small sex-specific effects.

Table 1. G×S interactions inferred through sex-specific window variances. Listed are loci with at least 0.95 posterior probability that sex-specific window variances differ. The table is sorted first by trait, then by magnitude of the female-specific window variance. Results are filtered such that each window listed consisted of a distinct set of SNPs. A full list of all G×S signals at a PPDiff$_{\sigma^2_{g_{j^*}}} \geq 0.90$ threshold is provided in S2 Table.

Focal SNP[a]	trait	$\hat{\sigma}^2_{g_{m_{j^*}}}$ [b]	$\hat{\sigma}^2_{g_{f_{j^*}}}$ [b]	PPM$_{\sigma^2_{g_{j^*}}}$	PPF$_{\sigma^2_{g_{j^*}}}$	PPDiff$_{\sigma^2_{g_{j^*}}}$	Nearest gene[c]	location	eQTL[d]
rs8176719	BMD	0.06000	0.00182	1.000	0.794	1.000	*ABO*	exon/frameshift	yes
rs1535515	height	0.00211	0.01170	0.819	0.999	0.956	*LRRC8C*	intron	yes
rs1544926	height	0.00763	0.00035	0.983	0.418	0.955	*COL23A1*	UTR-3	yes
rs6905288	WHR	0.00567	0.22200	0.920	1.000	1.000	***VEGFA***	downstream	
rs72961013	WHR	0.03260	0.18100	1.000	1.000	1.000	***RSPO3***	downstream	
rs1128249	WHR	0.00132	0.10700	0.614	1.000	1.000	***COBLL1***	intron	yes
rs12022722	WHR	0.00080	0.07180	0.490	1.000	1.000	***LYPLAL1***	downstream	yes
rs1776897	WHR	0.00870	0.06140	0.976	1.000	0.950	***HMGA1***	upstream	yes
rs11057401	WHR	0.00438	0.06030	0.846	1.000	1.000	***CCDC92***	exon/missense	yes
rs17777180	WHR	0.00031	0.05950	0.291	1.000	1.000	***CMIP***	intron	yes
rs4607103	WHR	0.00195	0.05920	0.809	1.000	1.000	***ADAMTS9-AS2***	intron	yes
rs6937293	WHR	0.00457	0.04660	0.839	1.000	1.000	***LOC728012***	downstream	yes
rs16861373	WHR	0.00066	0.04300	0.389	1.000	0.995	***PLXND1***	intron	
rs73068463	WHR	0.00068	0.04220	0.461	1.000	1.000	***SNX10***	intron	yes
rs9376422	WHR	0.00107	0.04180	0.524	1.000	1.000	*LOC645434*	upstream	
rs6867983	WHR	0.00192	0.03820	0.440	1.000	0.998	***MAP3K1***	upstream	
rs2171522	WHR	0.00241	0.03650	0.561	1.000	0.998	***ITPR2***	downstream	yes
rs3810068	WHR	0.00026	0.03590	0.174	1.000	1.000	*EMILIN2*	upstream	yes
rs568890	WHR	0.00129	0.03110	0.809	1.000	1.000	***NKX2-6***	upstream	yes
rs1332955	WHR	0.00647	0.02940	0.970	1.000	0.973	***LOC284688***	downstream	yes
rs13133548	WHR	0.00019	0.02400	0.175	0.969	0.956	***FAM13A***	intron	yes
rs11263641	WHR	0.00207	0.02340	0.723	1.000	0.991	*MYEOV*	downstream	yes
rs2800999	WHR	0.00201	0.02220	0.691	1.000	0.979	*TSHZ2*	intron	
rs2244506	WHR	0.00101	0.02070	0.453	0.998	0.985	*MIR5694*	downstream	
rs7259285	WHR	0.00182	0.01710	0.767	1.000	0.989	*HAUS8*	downstream	yes
rs4450871	WHR	0.00002	0.01680	0.027	1.000	1.000	*CYTL1*	downstream	
rs4080890	WHR	0.00153	0.01630	0.594	0.999	0.975	***KCNJ2***	downstream	
rs4684859	WHR	0.00039	0.01570	0.330	0.998	0.994	***PPARG***	downstream	
rs7704120	WHR	0.00049	0.01370	0.476	0.998	0.991	*STC2*	downstream	
rs10991417	WHR	0.00048	0.01230	0.339	0.986	0.966	*ABCA1*	intron	yes
rs12454712	WHR	0.00087	0.01020	0.360	0.996	0.965	***BCL2***	intron	yes
rs62070804	WHR	0.00004	0.00887	0.052	0.969	0.961	*ABHD15*	exon/missense	yes
rs10760322	WHR	0.00027	0.00812	0.282	0.986	0.968	*LHX2*	downstream	
rs1361024	WHR	0.00022	0.00760	0.203	0.982	0.962	*ESR1*	intron	
rs1358503	WHR	0.00021	0.00716	0.309	0.989	0.966	*SEMA3C*	upstream	yes
rs13156948	WHR	0.00016	0.00660	0.079	0.970	0.957	*IRX1*	downstream	
rs12432376	WHR	0.01740	0.00074	1.000	0.552	0.994	*STXBP6*	upstream	

[a] Focal SNP is defined as the center SNP j in window j^*.

[b] Male- and female-specific window variances, expressed as a percentage.

[c] Nearest gene and location identified through Axiom UKB WCSG annotations, release 34. The gene/locus is bold if it has been previously detected as a G×S interaction for WHR or WHR adjusted for BMI [21–24].

[d] If "yes", the focal SNP is significantly associated with gene expression in at least one tissue, according to GTEx V7.

Additionally, we utilized a traditional SMR approach (see Methods) for the discovery of G×S interactions among traits to compare *pvalue*-diff signals to PPDiff$_{\sigma^2_{g_{j^*}}}$ signals (S3 Fig). At

296 *pvalue*-diff $\leq 5\text{x}10^{-8}$, there were no genome-wide significant G×S-interacting SNPs for height,
297 one significant SNP for BMI nearby a window with $\text{PPDiff}_{\sigma^2_{g_{j^*}}} \geq 0.9$, and one significant peak
298 within *ABO* for BMD (the same signal detected using $\text{PPDiff}_{\sigma^2_{g_{j^*}}}$). Regions with a $\text{PPDiff}_{\sigma^2_{g_{j^*}}} \geq 0.9$
299 generally coincided with at least nominally-significant *pvalue*-diff signals; for height and BMD,
300 regions with $\text{PPDiff}_{\sigma^2_{g_{j^*}}} \geq 0.9$ also possessed a peak SNP with *pvalue*-diff ≤ 0.01. For BMI,
301 $\text{PPDiff}_{\sigma^2_{g_{j^*}}} \geq 0.9$ signals possessed a peak SNP of *pvalue*-diff ≤ 0.1. This, together with the fact
302 that novel G×S interactions found using LBR possess relatively small sex-specific effects,
303 suggests that LBR may be detecting G×S interactions that are otherwise missed due to low
304 power. Lastly for WHR, most of the high-confidence $\text{PPDiff}_{\sigma^2_{g_{j^*}}} \geq 0.9$ signals coincided with clear
305 and obvious *pvalue*-diff peaks.
306

307 **Inferred G×S interactions are enriched in tissue-specific eQTL**

308 As seen previously, many G×S interactions inferred using LBR have exceedingly small
309 sex-specific effects. To further investigate whether G×S detections using the $\text{PPDiff}_{\sigma^2_{g_{j*}}}$ metric
310 may be functionally relevant, we inferred whether such signals are enriched in eQTL identified
311 from GTEx. Specifically, using a hypergeometric test we asked whether $\text{PPDiff}_{\sigma^2_{g_{j^*}}}$-selected
312 focal SNPs (SNP j within window j^*) were enriched in eQTL, then compared to eQTL
313 enrichment from *pvalue*-diff-selected SNPs as a function of the number of SNPs selected (S4
314 Fig). $\text{PPDiff}_{\sigma^2_{g_{j^*}}}$-selected focal SNPs showed consistently higher eQTL enrichment than *pvalue*-
315 diff-selected SNPs for all traits except WHR. For instance, at $\text{PPDiff}_{\sigma^2_{g_{j^*}}} \geq 0.9$, the total number

316 of windows (focal SNPs) selected was 36, 264, 34, and 13, for height, WHR, BMD, and BMI,
317 respectively. With these selections, eQTL enrichment *p*-values were $2.39x10^{-4}$, $1.52x10^{-12}$,
318 $2.01x10^{-12}$, and $8.33x10^{-4}$, for height, WHR, BMD, and BMI, respectively. When selecting the
319 same number of SNPs using *pvalue*-diff, enrichment *p*-values were $2.25x10^{-2}$, $1.56x10^{-28}$,
320 $5.54x10^{-8}$, 1.93^{-1}, for height, WHR, BMD, and BMI, respectively.

321 To provide more information about how genetic regions bearing G×S interactions may
322 impact gene expression in specific tissues, we determined whether focal SNPs at $\text{PPDiff}_{\sigma^2_{g_{j*}}} \geq 0.9$
323 are enriched in tissue-specific eQTL (Fig. 5). For height, BMD, and WHR, such SNPs showed
324 significant eQTL enrichment in at least one tissue, using a conservative bonferroni corrected
325 enrichment *p*-value of $2.6x10^{-4}$ (correcting for 192 tests in total; 48 tissues and 4 traits).
326 Interestingly, BMD's G×S signals are very strongly enriched in eQTL with associated eGenes
327 (including *ABO* and *CYP3A5)* expressed in the adrenal gland, among other tissues. For height,
328 we observed small enrichment *p*-values across many tissues since G×S focal SNPs are enriched
329 in eQTL with associated eGenes (including *LOC101927975* and *CNDP2*) expressed across many
330 tissues. Lastly for WHR, we observed G×S detections to be heavily enriched in eQTL with
331 associated eGenes expressed in fibroblast, adipose, and skin tissues.
332

333 ## Discussion

334 We have investigated the degree to which sex-specific genetic architectures differ at local
335 regions, using large biobank data (N ~ 119,000 males and ~140,000 females) and Bayesian
336 multiple regression techniques that estimate sex-specific marker effects accounting for local LD
337 patterns. The flexibility of the Bayesian approach enables multi-resolution inference of sex-
338 specific effects: from individual SNP effects to window-variances that aggregate SNP effects

339 within chromosome segments. These inferences can be drawn all using the results of the same
340 model fit (eq. 1) but different post-processing of samples of SNP effects from the posterior
341 distribution.

342 The Bayesian multiple regression technique performed in this study, along with
343 estimation of window variances, was largely inspired by Fernando et al. [14]. In that study,
344 windows were defined using disjoint, fixed intervals. In contrast, for each SNP we define a
345 window based on local LD patterns, resulting in heavily overlapping, dynamically sized
346 windows. The methods presented here also bear resemblance to those of Vilhjálmsson et al. [18],
347 which utilized point-normal priors to estimate human SNP effects after accounting for local LD
348 patterns. In that study, posterior means of SNP effects were estimated for the purposes of
349 prediction while in this study, we numerically derive the full posterior distribution, allowing for
350 inference of non-null SNP effects and window variances.

351 Through simulations, we showed that local Bayesian regressions (LBR) provide superior
352 power and precision to detect causal variants and those specifically bearing G×S interactions. We
353 rationalize improvements in power upon traditional SMR methods by noting that the magnitude
354 of a typical causal variant or G×S interaction is exceedingly small and can elude hypothesis
355 testing partly due to the burden of multiple test correction. We also note that the resolution (peak
356 size) in SMR signals is relatively large when using large sample sizes (due to not fully
357 accounting for local LD patterns). To overcome this problem, we provided evidence that LBR
358 methods—either by estimating true marker effects or by aggregating true marker effects within
359 relatively small regions—can achieve improved resolution when working with large sample sizes
360 such as biobank-level data.

When using LBR to analyze real human traits, we have provided credence to our posterior probability-based discoveries by determining that LBR-detected G×S interactions are generally more enriched in eQTL than SMR-detected interactions. For BMD, we provided new evidence that sex-specific effects differ within *ABO* and that G×S interactions are highly enriched in adrenal gland-specific eQTL. This encourages the hypothesis that some G×S are eQTL that may modulate gene expression in the adrenal gland, with gene function dependent on the presence or absence of sex hormones. This was also an intriguing finding given that ABO blood groups have been known to associate with osteoporosis and osteoporosis severity [34,35]. For WHR, we detected previously known, large-magnitude G×S interactions that were discovered using WHR or WHRadjBMI [21–24], but additionally discovered novel, small magnitude G×S interactions near such genes as *ESR1* and *ABCA1*. In a previous work analyzing WHRadjBMI, *ABCA1* showed a significant female-specific genetic effect only, however the test for G×S interaction failed to reach significance [24].

For traits like height and BMI, large effect loci are estimated to have very similar effects between males and females and loci with evidence of G×S interactions were those possessing relatively small sex-specific effects. As seen in Fig 4B, many relatively large window variances for height are estimated to be slightly higher for males than for females albeit not reaching a $\text{PPDiff}_{\sigma^2_{g_{j^*}}} \geq 0.9$ threshold. This is consistent with the fact that the global genomic variance for height was estimated to be higher in males than in females in a previous study using the interim release of the UK Biobank [4]. Similarly, the same prior study estimated the global genomic variance of BMI to be higher in females than in males and we observe, if anything, evidence of sex-specific window variances leading to the same conclusion. These observations may potentially indicate that relatively large causal variants have slightly different sex-specific effects

for traits like height and BMI, however, if that is the case we are still underpowered to confidently detect such interactions.

It is important to acknowledge that while the methods presented here appear useful to decipher sex-specific genetic architectures from large human samples, additional work will be required to determine how these techniques may infer heterogeneous genetic effects in other contexts (other types of gene-by-covariate interactions), or when using different sample sizes or samples from different populations. With large sample sizes, the increased power and flexibility of the LBR comes with the cost of a significantly larger computational burden than the one involved in the traditional SMR approach; however, working with large datasets can be made manageable by adjusting size of each fitted segment (Fig 1) and parallel processing the fitting of each segment. Alternatively, LBR may be used as a follow up to traditional SMR tests, using pre-selected regions of interest. Another limitation inherent to aggregating SNP effects using window variances is that the sign of the effect is lost. In this way, when inferring G×S interactions through window variance differences, we cannot comment on whether sex-specific effects had the same sign or differing signs.

To conclude, we have demonstrated the powerful and flexible use of local Bayesian regressions for GWA to infer sex-specific genetic effects and G×S interactions using the UK Biobank. This was largely done by showing various means to utilize estimates of true (accounting for local LD), sex-specific SNP marker effects for GWA even when causal variants are not on the SNP panel for analysis. We anticipate that many more traits will be analyzed with this method to increasingly learn more about what is contributing to differences between males and females in human populations.

Methods

Genotype data

Individuals from the UK Biobank [36] were genotyped using the custom UK Biobank Axiom Array (http://www.ukbiobank.ac.uk/scientists-3/uk-biobank-axiom-array/) containing ~800,000 SNPs. SNP quality control proceeded with the Caucasian cohort (N = 409,700); SNPs with a minor allele frequency < 0.01 and missing call rate > 0.05 were removed. SNPs from sex chromosomes and the mitochondrial chromosome were not considered in this study, resulting in 607,497 autosomal SNPs. Individuals with coefficient of relatedness of 0.03 or greater were removed from analysis, resulting in 258,928 distantly related genotyped individuals for use in this study.

Phenotype data

All phenotypic data was collected using baseline measurements of UK Biobank participants. For height, the description “Standing height” from the UK Biobank was used. Individuals with heights (cm) less than 147 or more than 210 were removed from analysis. For BMD, the descriptions “Heel bone mineral density (BMD)”, “Heel bone mineral density (BMD) (left)”, and “Heel bone mineral density (BMD) (right)” were used in conjunction; for individuals with missing “Heel bone mineral density (BMD)” records, either the (left), the (right), or if available, the average between (left) and (right) was used. For BMI, the description “Body mass index (BMI)” was used and for WHR, the ratio of "Waist circumference” to “Hip circumference” was used. Prior to model fitting, all traits were pre-corrected for sex, age, batch, genotyping center, and the first 5 principle components derived from genomic data. The adjusted phenotypes

consisted of least-squares residuals from a model that included the effects listed above. For each trait, sample sizes and within-sex summary statistics are provided in S1 Table.

LBR hyperparameters

Hyperparameters used in the LBR model (eq. 1) were error variances for each sex, the proportion of nonzero effects for each SNP effect component, and the variances of nonzero effects for each SNP effect component $\{\sigma^2_{\mathrm{m}}, \sigma^2_{\mathrm{f}}, \pi_0, \pi_{\mathrm{m}}, \pi_{\mathrm{f}}, \sigma^2_{b_0}, \sigma^2_{b_{\mathrm{m}}}, \sigma^2_{b_{\mathrm{f}}}\}$. Variances (of either SNP effect components or sex-specific errors) were given a scaled-inverse Chi-square prior, parameterized by a degree of freedom parameter *df* (set to 5) and scaling parameter *S*. *S* is set according to built-in rules of the BGLR package using a prior model R-squared of 0.03 for main effects and 0.01 for the sex-interaction terms. More detail on how the scale parameter *S* is calculated can be found in Perez and de los Campos, 2014 [27]. π_k was given a beta prior with shape parameters $\alpha = 2$ and $\beta = 2$. An example of how to implement LBR (eq. 1) using BGLR with the above hyperparameter specifications is provided at https://github.com/funkhou9/LBR-sex-interactions.

Inference using post-processing of posterior samples

BGLR uses Markov chain Monte Carlo (MCMC) to sample from the posterior distribution of sex-specific effects. For each MCMC sample we derived male and female effects using $\beta_{\mathrm{m}_{j(s)}} = b_{0_{j(s)}} + b_{\mathrm{m}_{j(s)}}$ and $\beta_{\mathrm{f}_{j(s)}} = b_{0_{j(s)}} + b_{\mathrm{f}_{j(s)}}$, where s = 1,…, 4,350 indexes MCMC samples. Here, results were obtained using three separate MCMC chains. Each chain was

obtained using 3,400 MCMC samples; the first 500 samples were discarded as burn-in and the remaining samples where thinned by an interval of 2, leading to 1,450 samples per chain.

Estimates of sex-specific SNP effects ($\hat{\beta}_{\mathrm{m}_j}$ and $\hat{\beta}_{\mathrm{f}_j}$) were obtained from their posterior means. We estimated the posterior probability of a female-specific non-zero SNP effect using $\mathrm{PPF}_{\mathrm{SNP}_j} = \max\left[\Pr\left(\beta_{\mathrm{f}_j} > 0 \mid \mathcal{D}\right), \Pr\left(\beta_{\mathrm{f}_j} < 0 \mid \mathcal{D}\right)\right]$, where $\mathcal{D}$ represents the observed data. This was done by counting the proportion of β_{f_j} samples above zero and below zero. This was repeated for inferring the male-specific SNP effect. The posterior probability of sex-difference at individual SNP-effects was estimated using $\mathrm{PPDiff}_{\mathrm{SNP}_j} = \max\left[\Pr\left(\beta_{\mathrm{m}_j} > \beta_{\mathrm{f}_j} \mid \mathcal{D}\right), \Pr\left(\beta_{\mathrm{m}_j} < \beta_{\mathrm{f}_j} \mid \mathcal{D}\right)\right]$ where again these probabilities were estimated using the corresponding frequencies from the posterior distribution samples.

For each MCMC sample we also aggregated SNP effects within window j^* using $\boldsymbol{u}_{\mathrm{m}_{j^*(s)}} = \boldsymbol{X}_{j^*}\boldsymbol{\beta}_{\mathrm{m}_{j^*(s)}}$ and $\boldsymbol{u}_{\mathrm{f}_{j^*(s)}} = \boldsymbol{X}_{j^*}\boldsymbol{\beta}_{\mathrm{f}_{j^*(s)}}$. For this calculation we used a common genotype matrix $\boldsymbol{X}_{j^*}$ consisting of all N male and female genotypes to avoid differences in additive genetic values arising from allele frequency differences between males and females occurring by random sampling. Samples of sex-specific window variances were obtained using the sample variance: $\sigma^2_{g\,\mathrm{m}_{j^*(s)}} = (N-1)^{-1}\sum_{i=1}^{N}\left(u_{\mathrm{m}_{i\,j^*(s)}} - \bar{u}_{\mathrm{m}_{j^*(s)}}\right)^2$ and $\sigma^2_{g\,\mathrm{f}_{j^*(s)}} = (N-1)^{-1}\sum_{i=1}^{N}\left(u_{\mathrm{f}_{i\,j^*(s)}} - \bar{u}_{\mathrm{f}_{j^*(s)}}\right)^2$. Estimates of sex-specific window variances were obtained from their posterior means. Inferring sex-specific window variances was done by estimating $\mathrm{PPM}_{\sigma^2_{g\,j^*}} = \Pr\left(\sigma^2_{g\,\mathrm{m}_{j^*}} > 0 \mid \mathcal{D}\right)$ and $\mathrm{PPF}_{\sigma^2_{g\,j^*}} = \Pr\left(\sigma^2_{g\,\mathrm{f}_{j^*}} > 0 \mid \mathcal{D}\right)$ and inferring a G×S interaction at window j^* was done by estimating:

$$\text{PPDiff}_{\sigma^2_{g_{j*}}} = \max\begin{bmatrix}\Pr\left(\sigma^2_{g_{\text{m}_{j^*}}} - \sigma^2_{g_{\text{f}_{j^*}}} > t_{j^*} \mid \mathcal{D}\right), \\ \Pr\left(\sigma^2_{g_{\text{m}_{j^*}}} - \sigma^2_{g_{\text{f}_{j^*}}} < t_{j^*} \mid \mathcal{D}\right)\end{bmatrix},$$

where t_{j^*} was used to exert judgment about how different sex-specific window variances must be to declare a meaningful G×S interaction. Here, t_{j^*} was one-tenth of the mean of all posterior samples of $\sigma^2_{g_{\text{m}_{j^*}}}$ and $\sigma^2_{g_{\text{f}_{j^*}}}$. Functions to process posterior samples to estimate and infer non-null sex-specific effects and G×S interactions is provided at https://github.com/funkhou9/LBR-sex-interactions.

Defining local, LD-based windows

To define SNPs contained within window j^*, a region of LD centered on SNP j, we collected all SNP j' immediately surrounding SNP j for which $Cor\left(\boldsymbol{x}_j, \boldsymbol{x}_{j'}\right)^2 \geq 0.1$. We allowed up to two consecutive SNPs in which $Cor\left(\boldsymbol{x}_j, \boldsymbol{x}_{j'}\right)^2 < 0.1$ to allow for potential mapping errors or other unexplained instances where LD with SNP j dips only briefly. The function `getWindows()`, which provides windows given a genotype matrix $\boldsymbol{X}$, is provided in https://github.com/funkhou9/LBR-sex-interactions.

Single marker regression

We also performed single-marker regression analyses using following model:

$$\begin{bmatrix}\boldsymbol{y}_{\text{m}} \\ \boldsymbol{y}_{\text{f}}\end{bmatrix} = \begin{bmatrix}\mathbf{1}\mu_{\text{m}} \\ \mathbf{1}\mu_{\text{f}}\end{bmatrix} + \begin{bmatrix}\boldsymbol{x}_{\text{m}_j} \\ \boldsymbol{x}_{\text{f}_j}\end{bmatrix}\beta_j + \begin{bmatrix}\boldsymbol{x}_{\text{m}_j} \\ \mathbf{0}\end{bmatrix}\beta_{j_{\text{G×S}}} + \begin{bmatrix}\boldsymbol{\varepsilon}_{\text{m}} \\ \boldsymbol{\varepsilon}_{\text{f}}\end{bmatrix}.$$

As with the LBR model (eq. 1), we assume sex-specific errors are distributed normally with zero mean and sex-specific variances. SNP effects and interactions were estimated using weighted least squares. To test for a G×S interaction at SNP *j*, a t-test is used: $\hat{\beta}_{j_{GxS}}/SE\left(\hat{\beta}_{j_{GxS}}\right) \sim t_{N-3}$. The *p*-value from such a test is referred to as *pvalue*-diff. To test for any association (either among males, females, or both), we used an F-test, comparing a restricted model: $\begin{bmatrix} y_{\mathrm{m}} \\ y_{\mathrm{f}} \end{bmatrix} = \begin{bmatrix} \mathbf{1}\mu_{\mathrm{m}} \\ \mathbf{1}\mu_{\mathrm{f}} \end{bmatrix} + \begin{bmatrix} \varepsilon_{\mathrm{m}} \\ \varepsilon_{\mathrm{f}} \end{bmatrix}$ against the unrestricted model: $\begin{bmatrix} y_{\mathrm{m}} \\ y_{\mathrm{f}} \end{bmatrix} = \begin{bmatrix} \mathbf{1}\mu_{\mathrm{m}} \\ \mathbf{1}\mu_{\mathrm{f}} \end{bmatrix} + \begin{bmatrix} x_{\mathrm{m}_j} \\ x_{\mathrm{f}_j} \end{bmatrix} \beta_j + \begin{bmatrix} x_{\mathrm{m}_j} \\ \mathbf{0} \end{bmatrix} \beta_{j_{\mathrm{G\times S}}} + \begin{bmatrix} \varepsilon_{\mathrm{m}} \\ \varepsilon_{\mathrm{f}} \end{bmatrix}$.

Simulations

Simulated traits were developed using 60,000 genotyped SNPs (the first 6,000 SNPs from the first ten chromosomes) from 119,190 males and 139,738 females. Using these SNP genotypes, each trait was simulated as follows:

1. A total of 150 causal variants (CVs) were randomly sampled from 60,000 SNPs.
    - Let $\boldsymbol{Z}_{\mathrm{m}} = \left\{z_{\mathrm{m}_{ik}}\right\}_{i=1,k=1}^{N_{\mathrm{m}}=119{,}190\,,q=150}$ and $\boldsymbol{Z}_{\mathrm{f}} = \left\{z_{\mathrm{f}_{ik}}\right\}_{i=1,k=1}^{N_{\mathrm{f}}=139{,}738,q=150}$ denote matrices of male and female genotypes at sampled CVs.
2. Additive CV effect sizes were randomly sampled from the gamma distribution. 90 CVs (those with homogenous effects) were sampled from $\mathrm{Gamma}(k = 10, \theta = 1)$ and were made negative with a probability of 0.5. Of the 60 CVs with differing sex-specific effects, 30 had nonzero effects in both sexes but with deferring magnitudes: at random one sex's effects were sampled from $\mathrm{Gamma}(k = 5, \theta = 1)$ and the other from $\mathrm{Gamma}(k = 20, \theta = 1)$. For the

remaining 30 CVs, at random one sex's effects were exactly zero while the other sex's effects were sampled from $\mathrm{Gamma}(k = 10, \theta = 1)$.

- Let $\boldsymbol{\gamma}_{\mathrm{m}} = \{\gamma_{\mathrm{m}_k}\}_{k=1}^{q=150}$ and $\boldsymbol{\gamma}_{\mathrm{f}} = \{\gamma_{\mathrm{f}_k}\}_{k=1}^{q=150}$ denote vectors of male-specific and female-specific CV effects, respectively, for all 150 CVs.

3. Error variances for males $\sigma^2_{\delta_{\mathrm{m}}}$ and females $\sigma^2_{\delta_{\mathrm{f}}}$ were adjusted such that the proportion of phenotypic variance explained by all QTL is 0.05 for both males and females (on the complete genome scale this corresponds to a heritability of about 0.5).
    - Let $\delta_{\mathrm{m}_i} \sim N\left(0, \sigma^2_{\delta_{\mathrm{m}}}\right)$ and $\delta_{\mathrm{f}_i} \sim N\left(0, \sigma^2_{\delta_{\mathrm{f}}}\right)$ denote residual error for the i^{th} male and i^{th} female.
4. Male traits $\boldsymbol{\phi}_{\mathrm{m}} = \{\phi_{\mathrm{m}_i}\}_{i=1}^{N_{\mathrm{m}}=119,190}$ and female traits $\boldsymbol{\phi}_{\mathrm{f}} = \{\phi_{\mathrm{f}_i}\}_{i=1}^{N_{\mathrm{f}}=139,738}$ were simulated from a linear combination of QTL genotypes plus a residual error: $\boldsymbol{\phi}_{\mathrm{m}} = \boldsymbol{Z}_{\mathrm{m}}\boldsymbol{\gamma}_{\mathrm{m}} + \boldsymbol{\delta}_{\mathrm{m}}$ and $\boldsymbol{\phi}_{\mathrm{f}} = \boldsymbol{Z}_{\mathrm{f}}\boldsymbol{\gamma}_{\mathrm{f}} + \boldsymbol{\delta}_{\mathrm{f}}$
5. Steps 1-4 are repeated for 30 Monte Carlo replicates.

Acknowledgments

Enrichment analysis performed in this manuscript was done using data from the Genotype-Tissue Expression (GTEx) Project. Single-tissue cis-eQTL data was downloaded from https://gtexportal.org/home/datasets on 02/01/19.

References

1. Weiss LA, Pan L, Abney M, Ober C. The sex-specific genetic architecture of quantitative

traits in humans. Nat Genet. 2006;38: 218–222. doi:10.1038/ng1726

2. Zillikens MC, Yazdanpanah M, Pardo LM, Rivadeneira F, Aulchenko YS, Oostra BA, et al. Sex-specific genetic effects influence variation in body composition. Diabetologia. 2008;51: 2233–2241. doi:10.1007/s00125-008-1163-0

3. Yang J, Bakshi A, Zhu Z, Hemani G, Vinkhuyzen AAE, Nolte IM, et al. Genome-wide genetic homogeneity between sexes and populations for human height and body mass index. Hum Mol Genet. 2015;24: 7445–7449. doi:10.1093/hmg/ddv443

4. Rawlik K, Canela-Xandri O, Tenesa A, Carrel L, Willard H, Rinn J, et al. Evidence for sex-specific genetic architectures across a spectrum of human complex traits. Genome Biol. Genome Biology; 2016;17: 166. doi:10.1186/s13059-016-1025-x

5. Lynch M WJ. Genetics and Analysis of Quantitative Traits. 1st ed. Sinauer Associates, Inc; 1998.

6. Liu C-T, Estrada K, Yerges-Armstrong LM, Amin N, Evangelou E, Li G, et al. Assessment of gene-by-sex interaction effect on bone mineral density. J Bone Miner Res. 2012;27: 2051–64. doi:10.1002/jbmr.1679

7. Hoffmann TJ, Ehret GB, Nandakumar P, Ranatunga D, Schaefer C, Kwok PY, et al. Genome-wide association analyses using electronic health records identify new loci influencing blood pressure variation. Nat Genet. 2017;49: 54–64. doi:10.1038/ng.3715

8. Meuwissen THE, Hayes BJ, Goddard ME. Prediction of total genetic value using genome-wide dense marker maps. Genetics. 2001;157: 1819–1829. doi:11290733

9. de los Campos G, Sorensen D, Gianola D. Genomic Heritability: What Is It? PLoS Genet. 2015;11: 1–21. doi:10.1371/journal.pgen.1005048

10. Yang J, Benyamin B, McEvoy BP, Gordon S, Henders AK, Nyholt DR, et al. Common SNPs explain a large proportion of the heritability for human height. Nat Genet. 2010;42: 565–569. doi:10.1038/ng.608

11. Campos GDL, Gianola D, Allison DB. Predicting genetic predisposition in humans: the promise of whole-genome markers. Nat Publ Gr. Nature Publishing Group; 2010;11: 880–886. doi:10.1038/nrg2898

12. de los Campos G, Vazquez AI, Fernando R, Klimentidis YC, Sorensen D. Prediction of Complex Human Traits Using the Genomic Best Linear Unbiased Predictor. PLoS Genet. 2013;9. doi:10.1371/journal.pgen.1003608

13. Avery SG, Tellier L, Vazquez AI, de los Campos G, Lello L, Hsu SDH. Accurate Genomic Prediction of Human Height. Genetics. 2018;210: 477–497. doi:10.1534/genetics.118.301267

14. Fernando R, Toosi A, Wolc A, Garrick D, Dekkers J. Application of Whole-Genome Prediction Methods for Genome-Wide Association Studies: A Bayesian Approach. J Agric Biol Environ Stat. Springer US; 2017;22: 172–193. doi:10.1007/s13253-017-0277-6

15. Ayers KL, Cordell HJ. SNP Selection in genome-wide and candidate gene studies via penalized logistic regression. Genet Epidemiol. 2010;34: 879–891. doi:10.1002/gepi.20543

16. Yi N, George V, Allison DB. Stochastic Search Variable Selection for Identifying Multiple Quantitative Trait Loci. Genetics. 2003;164: 1129 LP – 1138. Available: http://www.genetics.org/content/164/3/1129.abstract

17. Zeng J, Pszczola M, Wolc A, Strabel T, Fernando RL, Garrick DJ, et al. Genomic breeding value prediction and QTL mapping of QTLMAS2011 data using Bayesian and GBLUP methods. BMC Proc. BioMed Central Ltd; 2012;6: S13. doi:10.1186/1753-6561-6-S2-S7

18. Vilhjálmsson BJ, Yang J, Finucane HK, Gusev A, Lindström S, Ripke S, et al. Modeling Linkage Disequilibrium Increases Accuracy of Polygenic Risk Scores. Am J Hum Genet. 2015;97: 576–592. doi:10.1016/j.ajhg.2015.09.001

19. de los Campos G, Veturi Y, Vazquez AI, Lehermeier C, Pérez-Rodríguez P. Incorporating Genetic Heterogeneity in Whole-Genome Regressions Using Interactions. J Agric Biol Environ Stat. Springer US; 2015;20: 467–490. doi:10.1007/s13253-015-0222-5

20. Veturi Y, de los Campos G, Yi N, Huang W, Vazquez AI, Kühnel B. Modeling heterogeneity in the genetic architecture of ethnically diverse groups using random effect interaction models. Genetics. 2019;(accepted): 1–13.

21. Heid IM, Jackson AU, Randall JC, Winkler TW, Qi L, Steinthorsdottir V, et al. Meta-analysis identifies 13 new loci associated with waist-hip ratio and reveals sexual dimorphism in the genetic basis of fat distribution. Nat Genet. 2010;42: 949–960. doi:10.1038/ng.685

22. Randall JC, Winkler TW, Kutalik Z, Berndt SI, Jackson AU, Monda KL, et al. Sex-

588 stratified Genome-wide Association Studies Including 270,000 Individuals Show Sexual
589 Dimorphism in Genetic Loci for Anthropometric Traits. Gibson G, editor. PLoS Genet.
590 2013;9: e1003500. doi:10.1371/journal.pgen.1003500

591 23. Winkler TW, Justice AE, Graff M, Barata L, Feitosa MF, Chu S, et al. The Influence of
592 Age and Sex on Genetic Associations with Adult Body Size and Shape: A Large-Scale
593 Genome-Wide Interaction Study. Adeyemo A, editor. PLOS Genet. 2015;11: e1005378.
594 doi:10.1371/journal.pgen.1005378

595 24. Shungin D, Winkler TW, Croteau-Chonka DC, Ferreira T, Locke AE, Mägi R, et al. New
596 genetic loci link adipose and insulin biology to body fat distribution. Nature. 2015;518:
597 187–196. doi:10.1038/nature14132

598 25. Karasik D, Ferrari SL. Contribution of gender-specific genetic factors to osteoporosis risk.
599 Ann Hum Genet. 2008;72: 696–714. doi:10.1111/j.1469-1809.2008.00447.x

600 26. Habier D, Fernando RL, Kizilkaya K, Garrick DJ. Extension of the bayesian alphabet for
601 genomic selection. BMC Bioinformatics. 2011;12. doi:10.1186/1471-2105-12-186

602 27. Pérez P, De Los Campos G. Genome-wide regression and prediction with the BGLR
603 statistical package. Genetics. 2014;198: 483–495. doi:10.1534/genetics.114.164442

604 28. Sanna S, Jackson AU, Nagaraja R, Willer CJ, Chen WM, Bonnycastle LL, et al. Common
605 variants in the GDF5-UQCC region are associated with variation in human height. Nat
606 Genet. 2008;40: 198–203. doi:10.1038/ng.74

607 29. Correa-Rodríguez M, Rio-Valle JS, Rueda-Medina B. AKAP11 gene polymorphism is

associated with bone mass measured by quantitative ultrasound in young adults. Int J Med Sci. 2018;15: 999–1004. doi:10.7150/ijms.25369

30. Zhu D-L, Chen X-F, Hu W-X, Dong S-S, Lu B-J, Rong Y, et al. Multiple functional variants at 13q14 risk locus for osteoporosis regulate *RANKL* expression through long-range super-enhancer. J Bone Miner Res. 2018; doi:10.1002/jbmr.3419

31. Mullin BH, Walsh JP, Zheng HF, Brown SJ, Surdulescu GL, Curtis C, et al. Genome-wide association study using family-based cohorts identifies the WLS and CCDC170/ESR1 loci as associated with bone mineral density. BMC Genomics. BMC Genomics; 2016;17: 1–11. doi:10.1186/s12864-016-2481-0

32. Mullin BH, Zhao JH, Brown SJ, Perry JRB, Luan J, Zheng HF, et al. Genome-wide association study meta-analysis for quantitative ultrasound parameters of bone identifies five novel loci for broadband ultrasound attenuation. Hum Mol Genet. 2017;26: 2791–2802. doi:10.1093/hmg/ddx174

33. Locke AE, Kahali B, Berndt SI, Justice AE, Pers TH, Day FR, et al. Genetic studies of body mass index yield new insights for obesity biology. Nature. 2015;518: 197–206. doi:10.1038/nature14177

34. Choi JW, Pai SH. Associations between ABO blood groups and osteoporosis in postmenopausal women. Ann Clin Lab Sci. 2004;34: 150–153.

35. Lu BB, Li KH. Association between ABO blood groups and osteoporosis severity in Chinese adults aged 50 years and over. J Int Med Res. 2011;39: 929–933. doi:10.1177/147323001103900327

36. Sudlow C, Gallacher J, Allen N, Beral V, Burton P, Danesh J, et al. UK Biobank: An Open Access Resource for Identifying the Causes of a Wide Range of Complex Diseases of Middle and Old Age. PLOS Med. 2015;12: e1001779. doi:10.1371/journal.pmed.1001779

Supporting information

S1 Fig. LD statistics across distances.

S2 Fig. Estimated power and false-discovery rate for discovering observed SNPs with effects in at least one sex. Estimated power (left) and FDR (right) shown as a function of the number of SNPs selected. Each point represents a sample average and error bars represent 95% confidence intervals, each derived using 30 Monte Carlo replicates. LBR (SNP): local Bayesian regression, utilizing $\mathrm{PP}_{\mathrm{SNP}_j}$. SMR: single-marker regression, utilizing the F-test-based *p*-value.

S3 Fig. Power vs false-discovery rate for discovering genomic regions containing masked causal variants. Here power is defined as the expected proportion of causal variants that are being tagged by at least one selected SNP j or window j^*. False discovery rate is defined as the proportion of selected SNPs or windows that are not tagging any causal variants. Each point is an estimate and error bars for both axes represent 95% confidence intervals. Point estimates and intervals were derived using 30 Monte Carlo replicates. Each facet corresponds to a different "target area", a fixed width around each causal variant that defines the set of SNPs effectively tagging it. LBR (SNP): uses the $\mathrm{PP}_{\mathrm{SNP}_j}$ metric spanning 1-0. LBR (Window): uses the maximum

650 between $\mathrm{PPM}_{\sigma^2_{\tilde{g}_{j^*}}}$ and $\mathrm{PPF}_{\sigma^2_{\tilde{g}_{j^*}}}$ spanning 1-0. SMR: uses the F-test-based *p*-value spanning (on

651 the $-\log_{10}$ scale) 30-0.

652 **S4 Fig. Comparison between SMR and LBR for discovering G×S interactions.** Manhattan

653 plot showing *pvalue*-diff for each analyzed SNP. SNPs are colored yellow if they were focal

654 SNPs with a $\mathrm{PPDiff}_{\sigma^2_{\tilde{g}_{j^*}}} \geq 0.9$ and colored red if they were focal SNPs with a $\mathrm{PPDiff}_{\sigma^2_{\tilde{g}_{j^*}}} \geq 0.95$.

655 The dashed horizontal lines denote *p*-diff thresholds of $1\text{x}10^{-5}$ and $5\text{x}10^{-8}$.

656 **S5 Fig. eQTL enrichment as a function of the number of SNPs selected.** LBR (Window):

657 uses the $\mathrm{PPDiff}_{\sigma^2_{\tilde{g}_{j^*}}}$ metric. SMR: uses the *pvalue*-diff metric.

658 **S1 Table. Sex-specific phenotype statistics.** Height units: cm, BMD units: g/cm2, BMI units:

659 Kg/m2.

660 **S2 Table. Inferred G×S interactions using sex-specific window variances.** Listed are all

661 windows with a $\mathrm{PPDiff}_{\sigma^2_{\tilde{g}_{j^*}}} \geq 0.9$.

662

663

664

665

666

667

668

669

670

671

672 **Fig 1. Strategy for implementing local Bayesian regressions genome-wide**. The phenotype is
673 regressed upon multiple sequential SNPs using a sliding window approach. The core region
674 contained 1500 SNPs (roughly 8Mb, on average) and each buffer region contained 250 SNPs
675 (roughly 1Mb, on average). Core parameters (posterior samples) are stitched together, then sex-
676 specific effects and G×S interactions are inferred at the level of SNP *j* and window *j**.
677 **Fig 2. Estimated power and false-discovery rate for discovering observed SNPs with G×S**
678 **interactions.** Shown as a function of the number of SNPs selected. Each point represents a
679 sample average and error bars represent 95% confidence intervals, each derived using 30 Monte
680 Carlo replicates. LBR (SNP): local Bayesian regression, utilizing $\text{PPDiff}_{\text{SNP}_j}$. SMR: single-
681 marker regression, utilizing *pvalue*-diff.
682 **Fig 3. Power vs false-discovery rate for discovering genomic regions containing masked**
683 **G×S interactions.** Here power is defined as the expected proportion of G×S interactions that are
684 being tagged by at least one selected SNP *j* or window j^*. False discovery rate is defined as the
685 expected proportion of selected SNPs or windows that are not tagging any G×S interactions.
686 Each point is an estimate and error bars for both axes represent 95% confidence intervals. Point
687 estimates and intervals were derived using 30 Monte Carlo replicates. Each facet corresponds to
688 a different "target area", a fixed width around each G×S interaction that defines the set of SNPs
689 effectively tagging it. LBR (SNP): uses the $\text{PPDiff}_{\text{SNP}_j}$ metric spanning 1-0. LBR (Window):
690 uses the $\text{PPDiff}_{\sigma^2_{g_{j^*}}}$ metric spanning 1-0. SMR: uses the *pvalue*-diff metric spanning (on the -
691 $\log_{10}$ scale) 8-0.
692 **Fig 4. Comparing sex-specific genetic effects. (A)** Plot of estimated female SNP effects against
693 estimated male SNP effects for all 607,497 genotyped autosomal SNPs. Points are colored by
694 their posterior probability of sex difference at the level of individual SNPs. **(B)** Plot of estimated

695 female window variances against estimated male window variances for all 607,497 LD-based
696 windows, with each window j^* centered on a different focal SNP *j*. Points are colored by their
697 posterior probability of sex difference at the level of window variances. **(C)** Miami-like plot
698 depicting location and magnitude of G×S interactions identified through sex-specific window
699 variances. For each trait, showing estimated male window variance above the x-axis and
700 estimated female window variance below the x-axis. Vertical lines denote changing
701 chromosomes. A sample of windows is labeled with nearest gene annotation, obtained from
702 Axiom UKB WCSG annotations, release 34. Gray labels indicate nearest genes with relatively
703 large window variances evidently shared across sexes, while red labels indicate nearest genes
704 with detected G×S interactions.
705 **Fig 5. Evidence that LBR-identified G×S interactions are enriched in tissue-specific eQTL.**
706 Plotted on the x-axis is the *p*-value obtained from a hypergeometic test providing evidence that
707 focal SNPs selected using $\text{PPDiff}_{\sigma^2_{\tilde{g}_{j^*}}} \geq 0.9$ are enriched in tissue-specific eQTL. The dashed line
708 represents a Bonferroni corrected significance threshold of $2.6\text{x}10^{-4}$.
709

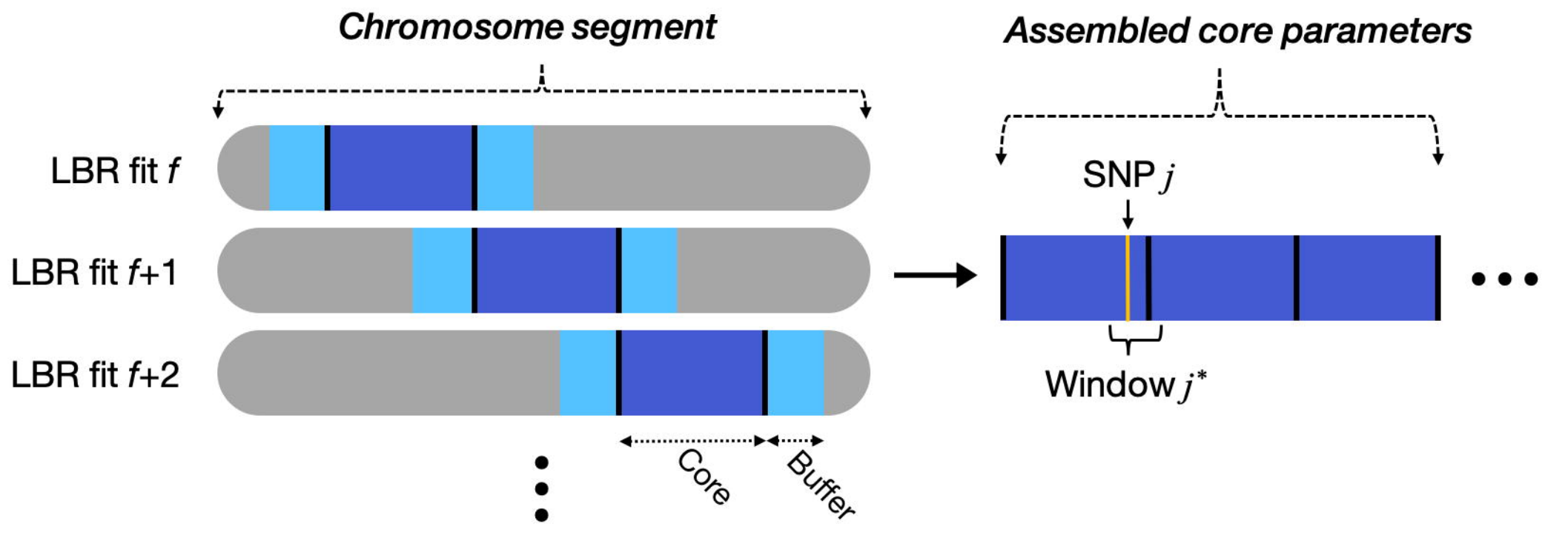
Chromosome segment
Assembled core parameters
LBR fit f
LBR fit f+1
LBR fit f+2
Core
Buffer
SNP j
Window j*

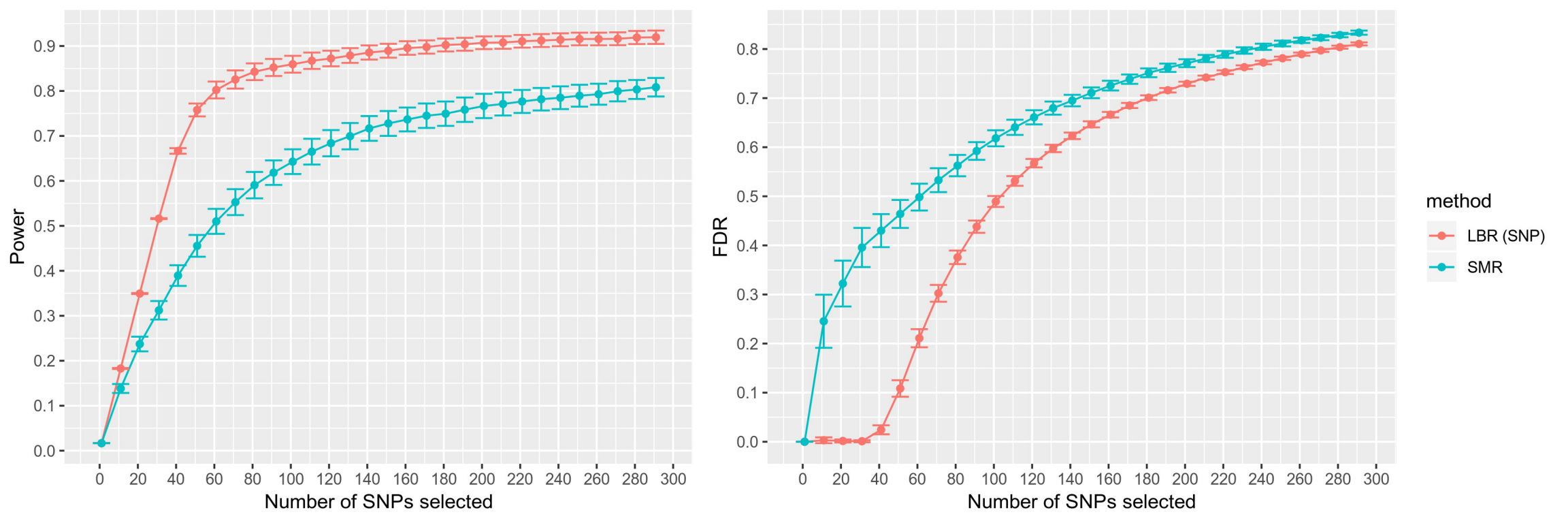
Power
0.0
0.1
0.2
0.3
0.4
0.5
0.6
0.7
0.8
0.9
0 20 40 60 80 100 120 140 160 180 200 220 240 260 280 300
Number of SNPs selected
FDR
0.0
0.1
0.2
0.3
0.4
0.5
0.6
0.7
0.8
0 20 40 60 80 100 120 140 160 180 200 220 240 260 280 300
Number of SNPs selected
method
LBR (SNP)
SMR

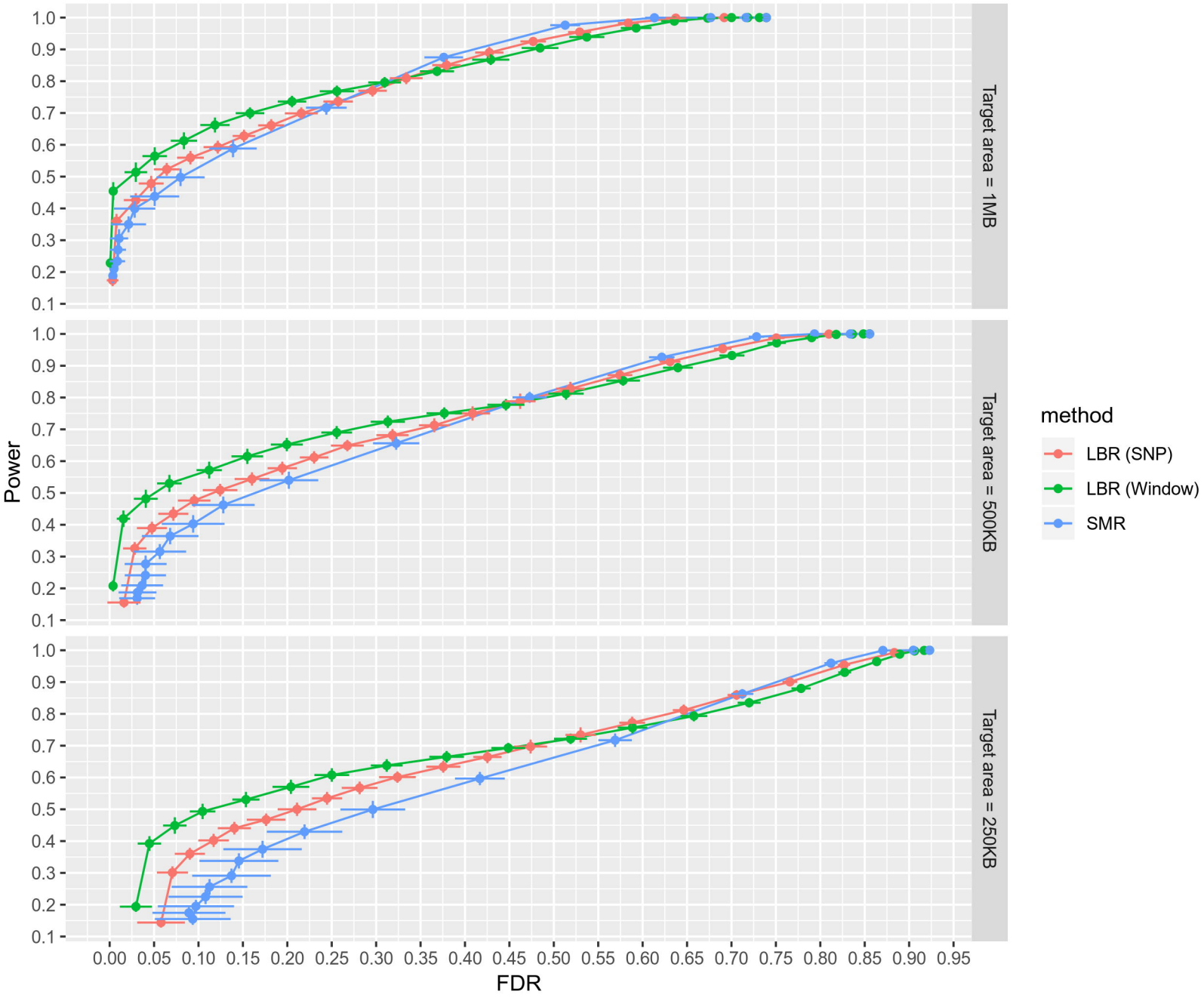
Power
FDR
Target area = 1MB
Target area = 500KB
Target area = 250KB
method
LBR (SNP)
LBR (Window)
SMR
1.0
0.9
0.8
0.7
0.6
0.5
0.4
0.3
0.2
0.1
0.00 0.05 0.10 0.15 0.20 0.25 0.30 0.35 0.40 0.45 0.50 0.55 0.60 0.65 0.70 0.75 0.80 0.85 0.90 0.95

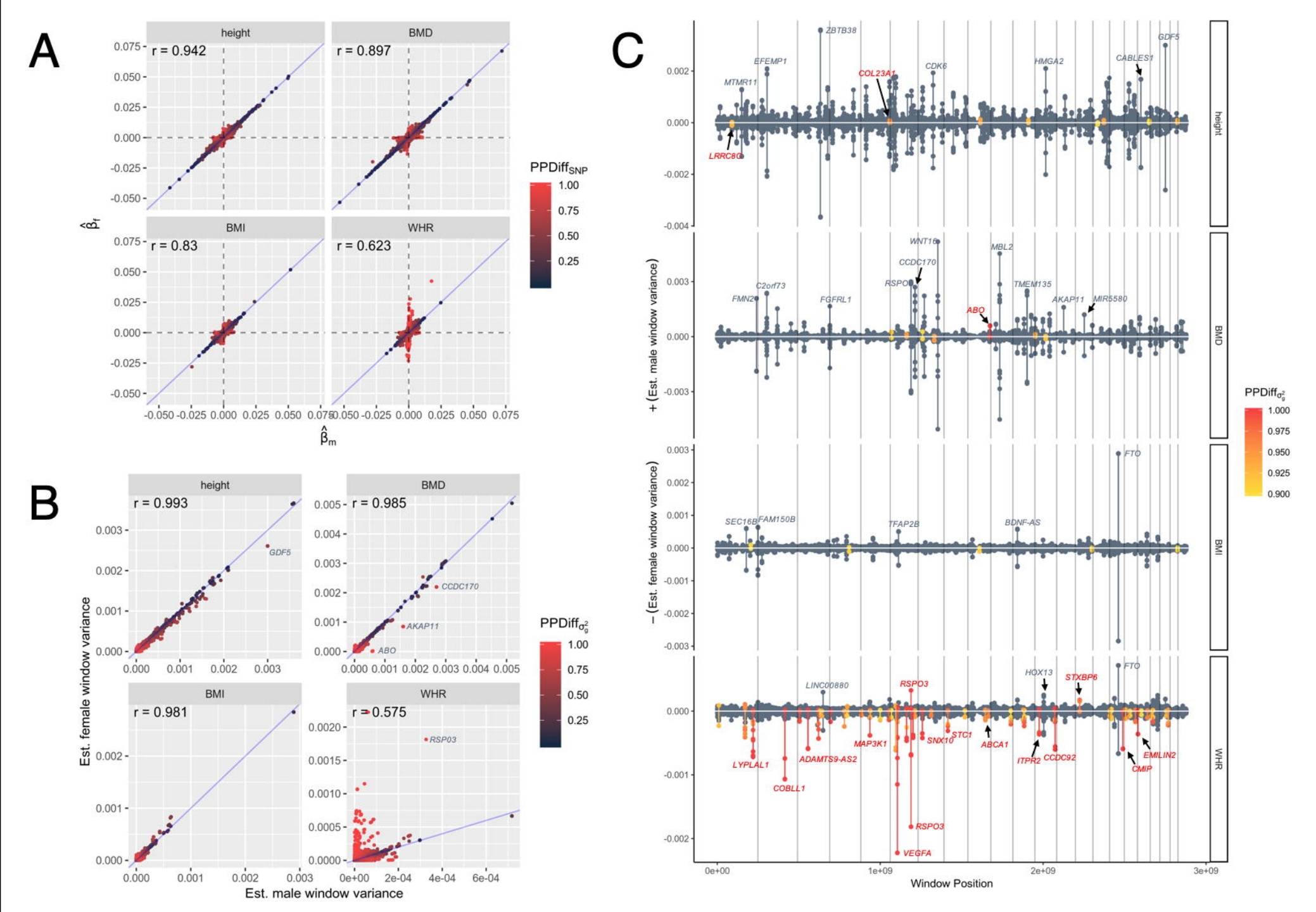
A
height
BMD
BMI
WHR
r = 0.942
r = 0.897
r = 0.83
r = 0.623
$\hat{\beta}_f$
$\hat{\beta}_m$
PPDiff$_{SNP}$
1.00
0.75
0.50
0.25
B
height
BMD
BMI
WHR
r = 0.993
r = 0.985
r = 0.981
r = 0.575
GDF5
CCDC170
AKAP11
ABO
RSPO3
Est. female window variance
Est. male window variance
PPDiff$_{\sigma^2_g}$
1.00
0.75
0.50
0.25
C
+ (Est. male window variance)
− (Est. female window variance)
ZBTB38
GDF5
EFEMP1
COL23A1
CDK6
HMGA2
CABLES1
MTMR11
LRRC8C
WNT16
MBL2
CCDC170
C2orf73
RSPO3
TMEM135
FMN2
FGFRL1
AKAP11
MIR5580
ABO
FTO
SEC16B
FAM150B
TFAP2B
BDNF-AS
LINC00880
RSPO3
HOXC13
STXBP6
FTO
MAP3K1
SNX10
STC1
ABCA1
ITPR2
CCDC92
EMILIN2
CMIP
LYPLAL1
ADAMTS9-AS2
COBLL1
RSPO3
VEGFA
Window Position
PPDiff$_{\sigma^2_g}$
1.000
0.975
0.950
0.925
0.900